Performance optimization of the CLIC positron source

Yongke Zhao,* Steffen Doebert, and Andrea Latina
CERN, Geneva, Switzerland

(Received 27 September 2024; accepted 3 January 2025; published 23 January 2025)

The baseline configuration of the Compact Linear Collider positron source is optimized at three different collision energy stages for both drive beam-based and klystron-based acceleration modes. The hybrid target is replaced with a single amorphous tungsten target with the target thickness and electron beam spot size optimized. As a result of the optimization, compared with the old baseline configuration, the positron yield has been improved by a factor of 1.65, enabling the same reduction in the bunch charge and beam power of the primary electron beam. The total deposited power in the target is reduced by a factor of 2.1. The most realistic start-to-end simulation to date of the system from the target to the injector linac is performed taking into account new design of essential hardware. The impact of misalignments is studied for the first time and is found to be small and acceptable. Possibility for reducing the primary electron beam energy is investigated. With a bunch charge below 1 nC, it is possible to reduce the energy from 5 GeV to a minimum of 2.3 GeV with the linac length and costs reduced accordingly. The deposited power in the target is also reduced with the energy.

DOI: 10.1103/PhysRevAccelBeams.28.011002

I. INTRODUCTION

The Compact Linear Collider (CLIC) [1,2] is a multi-TeV high-luminosity linear collider proposed to be built at the border of Switzerland and France, hosted by the European Organization for Nuclear Research (CERN). A novel two-beam acceleration technique with normal-conducting X-band accelerating structures has been developed, operating with a high average rf gradient in the range of 70 to 100 MV/m. The CLIC Conceptual Design Report (CDR) [1] was published in 2012. Three center-of-mass energy stages were proposed: 500 GeV, 1.5 TeV, and 3 TeV. However, the CDR was mainly focused on demonstrating the feasibility of the CLIC accelerator at 3 TeV. The CLIC Project Implementation Plan (PIP) report [2] was published in 2018, with high quality, very detailed documentation of baseline and alternative CLIC configurations. With the discovery of the Higgs boson in 2012, the first energy stage was then optimized and reduced to 380 GeV, which provides an excellent opportunity to perform precision measurements of the Standard Modelphysics processes, particularly in the Higgs and top-quark sectors. The higher energy stages provide opportunities to explore TeV-scale phenomena, such as the Higgs self-coupling and Beyond Standard Model physics.

To achieve the design performance, CLIC needs high-intensity electron and positron bunches. This paper focuses on the positron production scheme. The CLIC positron source must provide high-intensity and high-energy positron beams up to 2.86 GeV, which are then injected into the predamping ring (PDR) and damping ring (DR). The schematic layout of the optimized baseline design of the CLIC positron source is presented in Fig. 1. Positrons are generated with a 5 GeV electron beam from a thermionic electron gun and a driver linac impinging on a single amorphous tungsten target. The design of the electron gun and driver linac is not studied and discussed in this report. A pulsed tapered flux concentrator (FC) [3] is used as the adiabatic matching device (AMD), with an adiabatically decreasing magnetic field. The preinjector linac (PIL), composed of L-band traveling wave (TW) rf accelerating structures [4] and 0.5 T surrounding normal-conducting (NC) solenoids, will further capture and accelerate the positrons to about 200 MeV. Electrons and photons from the target are removed by a chicane and a collimator located at the PIL exit. The injector linac (IL) [5], which will be used for both electrons and positrons, will accelerate the positron beam to 2.86 GeV, with quadrupoles and the same L-band TW structures. At the PDR entrance, the longitudinal acceptance for the positron beam is considered by applying energy and time cuts. The PDR accepted positron yield is defined as the ratio of the number of positrons accepted by the PDR to the number of primary electrons.

Section II focuses on the start-to-end simulation and optimization of the CLIC positron source, from the target

*Contact author: yongke.zhao@cern.ch

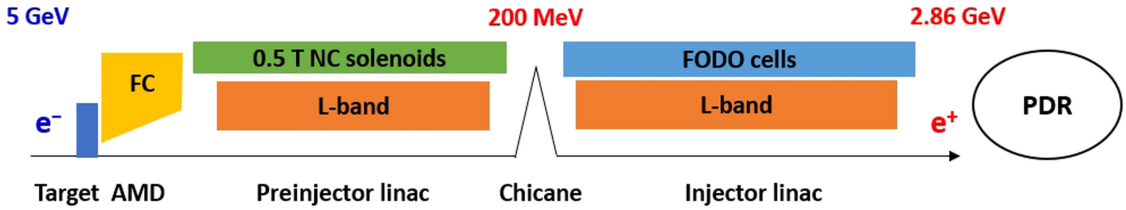

FIG. 1. Schematic layout of the latest baseline design for the CLIC positron source. Electron gun and driver linac are not inlcuded. AMD, adiabatic matching device; FC, flux concentrator; and PDR, predamping ring.

and primary electron beam to the end of the injector linac. The target scheme and the electron beam spot size are particularly optimized to maximize the PDR accepted positron yield. Significant improvements have been achieved in the realistic simulation of the system, involving the aperture and magnetic field of the AMD, the layout and magnetic field of the NC solenoids, the inclusion of the chicane and collimator, and the use of realistic rf field of the accelerating structures in the injector linac. The simulation results after optimization are presented in Sec. III. In Sec. IV, misalignments of the system are simulated and discussed. Section V presents a preliminary exploration of the possibility of reducing the primary electron beam energy and linac length.

II. THE CLIC POSITRON SOURCE

The target is simulated with Geant4 [6–8]. In the case of a hybrid target composed of crystal tungsten and amorphous tungsten, Fot [9,10], a simulation code developed mainly for photon production from the electron channeling process in crystal tungsten, is used. Fot uses the semiclassical Baier-Katkov formula [11] for radiation in a nonuniform field to calculate the electron trajectories in the crystal and subsequent photon emission probabilities, with the multiple scattering taken into account. An old crystal simulation code, called VMS [12], has been used for benchmarking for the hybrid target simulation, and the discrepancy is found to be 10%–20% [10]. The VMS code is no longer maintained and available. In recent years, Geant4 is also developing fast in terms of the crystal channeling simulation, and a model has been developed and applied to the FCC-ee positron source simulation [13–15]. Although the model is included in the latest Geant4 release, essential crystal potential field files are not available, and the application to other positron sources is still not feasible at the moment. The energy deposition in the target is estimated by creating a 3D cubic mesh around the target, with an optimized mesh grid size of 0.5 mm [16]. The peak energy deposition density (PEDD) is estimated by reading the maximum energy deposition in the mesh, scaled by the material density and the mesh volume. The PEDD is always normalized by the PDR accepted positron yield and the required bunch charge at the PDR entrance. The PEDD in the amorphous tungsten target is usually required to be less than 35 J/g, which has been experimentally approved to be the damage limit of tungsten at the Stanford Linear Collider after a 1000 days of operation [1]. rf-Track [17,18] is used to simulate the transport of the positron beam from the target to the PDR entrance.

To simplify the start-to-end simulation and optimization of the entire positron source, an analytic formula is usually used to calculate the energy gain of the positrons from the PIL exit to the PDR entrance:

$$\Delta E = (2.86\ \text{GeV} - E_{\text{ref}})\cos[2\pi f(t - t_{\text{ref}})], \qquad (1)$$

where E_{ref} and t_{ref} are the energy and time of the reference particle, which usually need to be optimized for a maximum PDR accepted positron yield, and $f = 2$ GHz is the L-band rf frequency. The time distribution at the PDR entrance in this case is the same as it is at the PIL exit. Such a manner to estimate the PDR accepted positron yield is called the "fast simulation" hereafter. Otherwise, it is called the "full simulation," where all elements are simulated. In the fast simulation, the chicane is also not simulated, and the magnetic field of the solenoids surrounding the PIL rf structures is replaced with a constant field of 0.5 T where necessary. This makes the fast simulation much faster than the full simulation, but the results are also less realistic and conservative. To be more conservative, when the fast simulation is used, the PEDD in the target is required to be less than 30 J/g instead of 35 J/g, taking into account the realistic losses of the positron yield. A comparison between the fast simulation and the full simulation is summarized in Table I.

A. Beam parameters

The primary electron beam is assumed to have a Gaussian distribution profile in the transverse and longitudinal phase

TABLE I. Comparison between fast simulation and full simulation.

Configuration	Fast simulation	Full simulation
NC solenoid	Uniform field	Analytic field
Chicane	Not considered	6D simulation
Injector linac	Analytic (longitudinal)	6D simulation
PEDD limit	30 J/g	35 J/g

TABLE II. Primary electron beam parameters and requirements for the positron beam at the PDR entrance after applying the PDR longitudinal acceptance cuts at different energy stages for different acceleration modes (DBA, drive beam-based acceleration and KBA, klystron-based acceleration). A 20% safety margin is already considered in the positron bunch charge.

Beam parameter	Unit	380 GeV		1.5 and 3 TeV
Acceleration mode		DBA	KBA	DBA
Electron beam				
Beam energy	GeV	5	5	5
Energy spread (σ_E/E)	%	0.1	0.1	0.1
Bunch length (σ_z)	mm	1	1	1
Spot size ($\sigma_{x,y}$)	mm	2.40	2.45	1.50
Normalized transverse emittance, $\epsilon^n_{x,y}$	mm mrad	80	80	80
Number of bunches per train		352	485	312
Positron beam				
Beam energy	GeV	2.86	2.86	2.86
Number of bunches per train		352	485	312
Bunch charge	nC	1.000	0.744	0.711
PDR energy acceptance (±)	%	1.2	1.2	1.2
PDR time cut window (total length)	mm/c	20	20	20

spaces without correlations. The latest baseline parameters of the electron beam and the requirements for the positron beam at the PDR entrance are summarized in Table II, at different energy stages for both drive beam-based (DBA) and klystron-based (KBA) acceleration modes. Each case has specified bunch charge and number of bunches with optimal overall luminosity performance. The electron transverse momentum spread, $\sigma_{P_{x,y}}$, is determined by the normalized transverse emittance, $\epsilon^n_{x,y}$, and the spot size, $\sigma_{x,y}$, which can be expressed with the following equation:

$$\epsilon^n_{x,y} = \frac{\sigma_{x,y}\sigma_{P_{x,y}}}{m_0 c}, \tag{2}$$

where m_0 is the electron rest mass. The electron spot size has been optimized to have a maximum PDR accepted positron yield and an acceptable PEDD in the target, as presented in Fig. 2. In the old baseline design and studies, a fixed electron spot size of 2.5 mm was used. The required bunch charge of the primary electrons is determined by the PDR accepted positron yield and the required positron bunch charge at the PDR entrance. After applying the PDR acceptance cuts, a 20% safety margin is considered in the positron bunch charge at the PDR entrance. To be conservative, the safety margin is slightly higher than the required margin in the CLIC CDR [1] and PIP report [2], where a 15% safety margin is assumed for the losses in the PDR and DR.

B. Target

In the CLIC PIP report published in 2018, a hybrid target has been used, which is composed of a thin crystal tungsten target of 1.4 mm and a thick amorphous tungsten target of 10 mm, with a distance of 2 m. The schematic layout of the hybrid target is displayed in Fig. 3. The crystal target is thought to be able to enhance photon production from the electron channeling process. A dipole with a magnetic field of 0.5 T is placed between the two targets to remove charged particles and reduce the PEDD in the amorphous target, as the PEDD in the amorphous target is usually much higher than the crystal target. In a report published in 2019 [19], the hybrid target has been optimized for a higher positron yield, focusing on the 3 TeV energy stage.

The advantage of using the hybrid target is that it is thought to significantly reduce the PEDD compared with the conventional single amorphous tungsten target. However, we have found that the PDR accepted positron yield of using the hybrid target is much lower than using a single amorphous tungsten target. This is mainly due to the

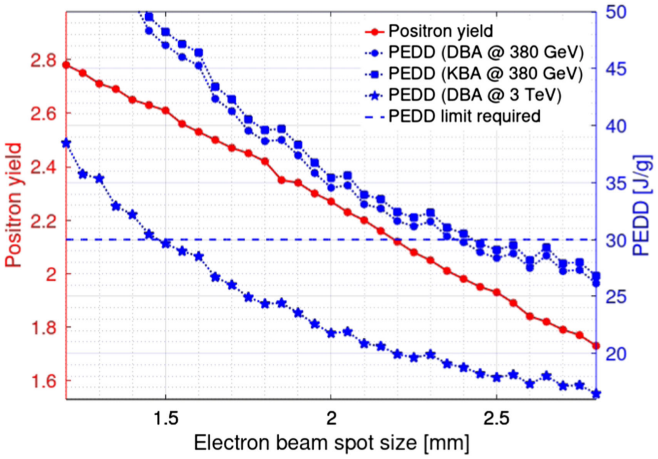

FIG. 2. Scan of the electron beam spot size. PDR accepted positron yield and normalized PEDD at different energy stages for different acceleration modes are plotted as a function of the spot size.

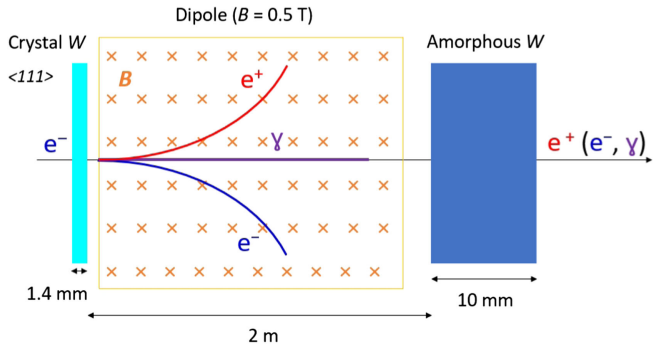

FIG. 3. Schematic layout of the hybrid target in the old baseline design, composed of a thin crystal tungsten and a thick amorphous tungsten. A dipole is supposed to be used between the targets to remove charged particles.

fact that the long distance between the crystal and the amorphous targets leads to a large positron beam size and low transport efficiency to the PDR. A scan of the hybrid target distance is presented in Fig. 4. The PDR accepted positron yield and the normalized PEDD in the amorphous target are estimated and plotted as a function of the distance between the crystal and amorphous targets. To simplify the study, the fast simulation is used in this case. Clearly it can be seen from the plot that the PDR accepted positron yield is increased significantly with a reduced distance, and the maximum yield is achieved when the distance is zero, which turns out to be a single target option. Even though the PEDD is also increased significantly with a reduced distance, it is still below 30 J/g, and it is possible to reduce the PEDD with an optimized target thickness and an increased electron beam spot size. Therefore, in the optimized baseline design, we use a single amorphous tungsten (W_{74}) target, with an optimized thickness of 18 mm, which gives much higher PDR accepted positron yield than the hybrid target option. Besides, the design, manufacturing, and mounting of the target will also be much easier. A scan of the target thickness for different beam energies and spot sizes is presented in Fig. 5. The PDR accepted positron yield is estimated and plotted as a function of the target thickness for different electron beam energies and spot sizes. At 5 GeV, which is the baseline electron beam energy, the optimized target thickness is about 18 mm.

A comparison of the target configuration and the final results between the old and optimized baselines is summarized in Table III at different energy stages for the DBA acceleration mode. To achieve a fair comparison, the same simulation code is used, and to simplify the study, the fast simulation is still used in this case. As a result of optimization, the final positron yield is significantly increased, and the electron bunch charge and beam power are significantly reduced. Compared with the most recently published optimization in 2019, the positron yield has been improved by a factor of 1.65, enabling the same reduction in the bunch charge and beam power of the primary electron beam. The total deposited power in the target is reduced by a factor of 2.1. Compared with the CLIC PIP report published in 2018, which is thought to be a very important roadmap for CLIC construction, the improvements are even more significant, as can be seen in this table. The design, manufacturing, and mounting of the new target scheme will also be much easier and conservative. Despite the significant improvements in the positron yield, the challenges in the sustainable operation of target have never been studied, such as the thermal load, radiation damage, and material fatigue. Even though a satisfied PEDD well below 35 J/g is achieved, the total deposited power in the target is still high. In this case, the cooling of the target might be a problem, especially for a fixed target. However,

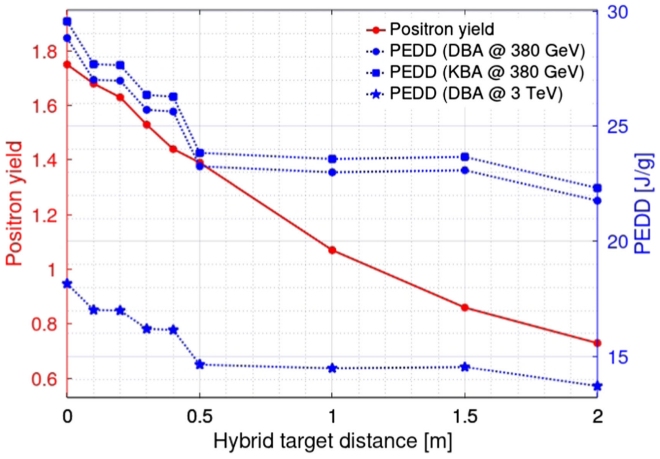

FIG. 4. Scan of the hybrid target distance in the old baseline design. PDR accepted positron yield and normalized PEDD at different energy stages for different acceleration modes are plotted as a function of the distance.

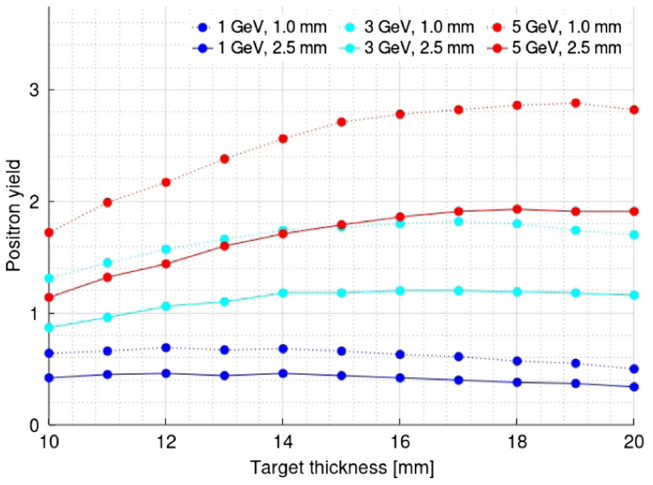

FIG. 5. Scan of the single target thickness in the new baseline design. PDR accepted positron yield is plotted as a function of the thickness for different beam energies and spot sizes.

TABLE III. Comparison of the old and optimized target configurations and fast simulation results at the 380 GeV energy stage (numbers in parentheses are for 1.5 and 3 TeV energy stages) for the DBA acceleration mode.

Parameter	Unit	PIP report in 2018	Report in 2019	Optimization
Electron beam energy	GeV	5	5	5
Electron beam spot size	mm	2.50	2.50 (1.25)	2.40 (1.50)
Required electron bunch charge	nC	1.37 (0.97)	0.83 (0.39)	0.51 (0.27)
Normalized electron beam power	kW	120.5 (76.0)	73.3 (30.3)	44.4 (21.2)
Target profile		Hybrid	Hybrid	Single
Target thickness	mm	1.4, 10	2.17 (1.68), 17.6 (14.9)	18
Hybrid target distance	m	2	0.67 (0.66)	…
Normalized PEDD in amorphous target	J/g	21.8 (13.7)	24.4 (25.6)	29.8 (29.6)
Normalized deposited power in amorphous target	kW	12.3 (7.7)	25.3 (8.2)	12.0 (5.7)
PDR accepted positron yield	e^+/e^-	0.73	1.20 (1.83)	1.98 (2.61)

a rotating target has been designed and studied for the International Linear Collider positron source, which is found to be able to provide a sufficient cooling with a even higher deposited power of 18.8 kW [20]. Similar solution can be applied to the CLIC positron source.

C. Adiabatic matching device

The Adiabatic Matching Device (AMD) is used to capture and improve the transport efficiency of the positrons with large divergence from the target. A strong peak on-axis magnetic field is usually required. The conventional way to achieve this is to use a pulsed normal-conducting (NC) flux concentrator (FC) with a tapered inner aperture. The maximum peak on-axis field that can be achieved by an FC is usually thought to be no larger than 6 T due to technical limitations.

In the old studies [1,2,19], the AMD was never designed, and a realistic magnetic field of the AMD was never used. A simple on-axis magnetic field has been assumed, as presented in Fig. 8, which is given by an adiabatic formula [21]:

$$B_z = \frac{B_0}{1+\mu z}, \tag{3}$$

where $B_0 = 6$ T is the peak on-axis field and $\mu = 55$ m^{-1} is an optimized scaling factor to shape the field. Besides, in the old studies, a constant inner aperture radius of 20 mm instead of a tapered aperture has been assumed in the simulations, which is not realistic and gives an overestimated positron yield.

In the new baseline and simulations, we use realistic aperture and 2D magnetic field for the AMD. A pulsed FC with a tapered aperture has been designed for the CLIC positron source, based on the SLAC FC design [22], and published earlier in a separate report, as detailed in Ref. [3]. Several options with linear and nonlinear inner aperture shapes have been explored in the design of the FC, and a linear aperture shape with the highest positron yield is adopted in this study. The inner aperture radius is increased linearly from 6.5 mm at the entrance to 55.45 mm at the exit. The outer radius is 60 mm. The total length of the FC is 127 mm. The gap between the target and the FC is assumed to be 2 mm. The design features 14 turns of copper coils with a total length of 127 mm. The turn width is 8.33 mm and the gap between the turns is 0.8 mm. The schematic layout of the AMD is displayed in Fig. 6. The current is pulsed in the form of a half-sine wave with a repetition rate of 25 kHz and a peak current of 20 kA. A 2D axi-symmetric modeling of the FC is performed with Opera-2D [23], and the 2D realistic field is computed and used for the positron beam tracking. As a result, a peak on-axis magnetic field of 6 T is achieved. The 2D field map of the FC is presented in Fig. 7, while the on-axis field is presented in Fig. 8, with a comparison with the analytic field used in old simulations. The prototype of the FC is being manufactured at CERN and is planned to be tested at the KEK test bench.

D. Preinjector linac

The Preinjector Linac (PIL) is placed downstream of the AMD and is used to further capture and accelerate the positrons to about 200 MeV. Similar design of the PIL as in

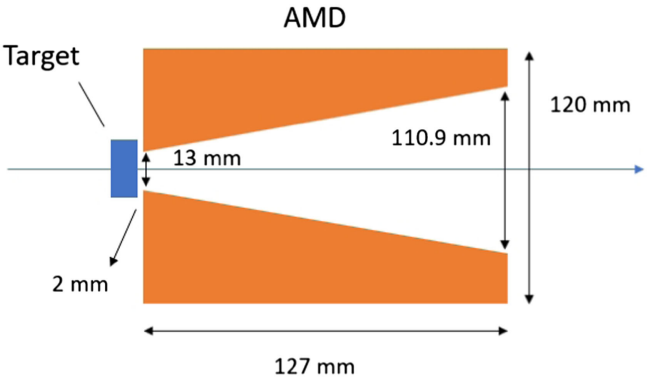

FIG. 6. Schematic layout of the AMD in the new baseline. An FC with a tapered aperture is used as the AMD, placed 2 mm downstream the target.

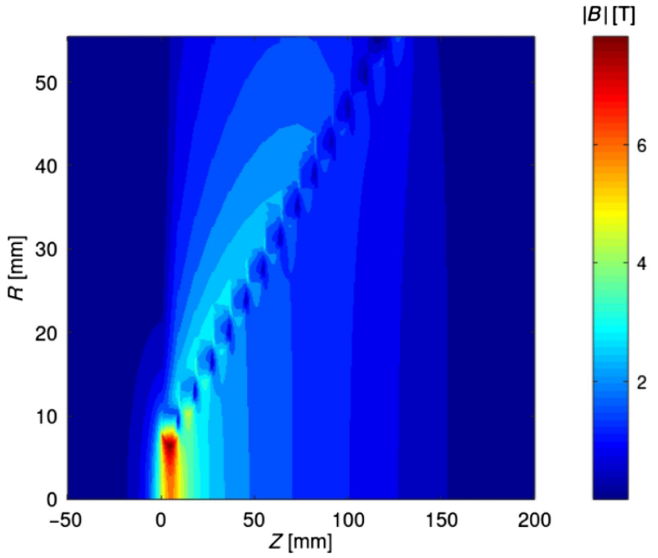

FIG. 7. 2D realistic magnetic field map of the FC, used as the AMD in the new baseline.

the old studies [19] is used. L-band TW structure [4], which is called the "CLIC L-band" structure, with an rf frequency of 2 GHz and a phase advance per cell of $2\pi/3$, is used. The structure is 1.5 m long and was designed mainly for the CLIC booster linac with a tapered iris radius from 20 to 14 mm. However, a constant iris radius of 20 mm is still assumed in our simulations for the positron source. The PIL comprises 11 TW structures, same as in the old studies [2,19], and is surrounded by NC solenoids, which are supposed to provide a uniform magnetic field of 0.5 T. To simplify the design, the distance between the structures is assumed to be always 20 cm, although it is found that the positron yield might be slightly increased by reducing the distance between the first two structures. To simplify

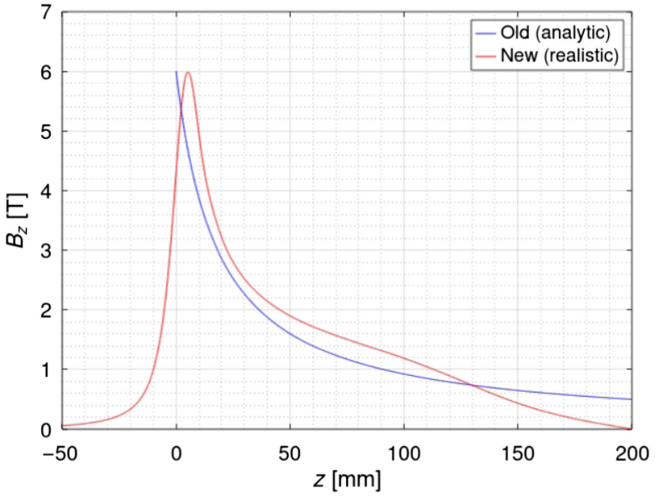

FIG. 8. Comparison between analytic and realistic on-axis magnetic fields of the AMD that are used in the old and new baselines, respectively.

the optimization, the average rf gradient is fixed to be 20 MV/m for all rf structures and two rf phases are optimized, with one phase for the first structure and one phase for the other structures. Using a higher gradient might be more challenging, even though the positron yield is found to be slightly increased with the gradient. It is found that the positron yield is not significantly increased by using more rf phases in the optimization, as the first structure plays the most important role in increasing the positron yield by reducing the bunch length. The rf phase in the first structure is optimized such that the head of the bunch is decelerated and the tail is accelerated. The other structures mainly accelerate the bunch with an optimized phase slightly off crest, such that the positron yield is maximized and the beam energy at the end of the PIL is around 200 MeV.

In the old studies, the layout of the NC solenoids has never been designed and considered. Instead, solenoids were always replaced with an on-axis field of 0.5 T, which is not realistic. In the new simulations, we use the following analytic formula [24] to describe the on-axis magnetic field of the NC solenoids:

$$B_z = \frac{\mu_0 NI}{2}\left(\frac{l/2-z}{l\sqrt{R^2+(l/2-z)^2}}+\frac{l/2+z}{l\sqrt{R^2+(l/2+z)^2}}\right), \tag{4}$$

where z is the longitudinal distance to the solenoid center, $\mu_0 = 4\pi \times 10^{-7}$ H/m is the vacuum magnetic permeability, N is the number of coils, I is the coil electric current, l is the length of the solenoid, and R is the average radius of the coils. Instead of specifying N and I of the coils, the field is scaled to a specific peak field, B_0, which is optimized to have a uniform field of 0.5 T surrounding the accelerating structures. For this purpose, three types of NC solenoids are assumed with different peak fields: (i) Type 0: Solenoid between the AMD and the first accelerating structure. A gap of 2 mm is assumed between the solenoid and the AMD or the structure. (ii) Type 1: Solenoid surrounding accelerating structures. Each structure is surrounded by seven solenoids with a total length of 1.38 m and a gap of 20 mm between solenoids. The center of the surrounding solenoids is the same as the structure. Coupler cells of the structure are not surrounded by solenoids. (iii) Type 2: Solenoid between accelerating structures. A gap of 10 mm is assumed between the solenoid and the structures. The different types of solenoids are summarized in Table IV.

TABLE IV. NC solenoids for the PIL.

Parameter	Symbol	Unit	Type 0	Type 1	Type 2
Average radius	R	mm	200	200	200
Length	l	mm	180	180	180
Peak field	B_0	T	0.38	0.23	0.31

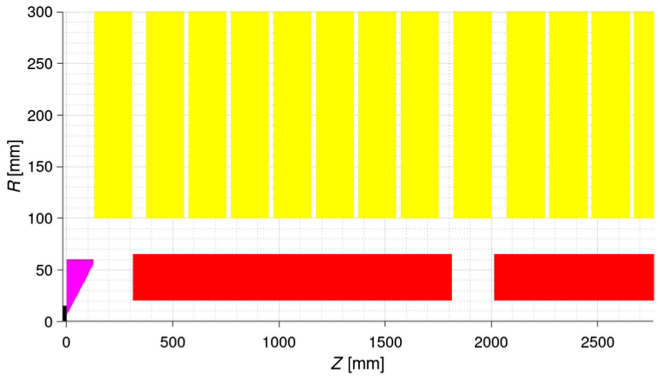

FIG. 9. Cross-sectional view of the schematic layout of the NC solenoids (in yellow), as well as the target (in black), AMD (in cyan), and accelerating structures (in red). Plot ranges are limited for a better display.

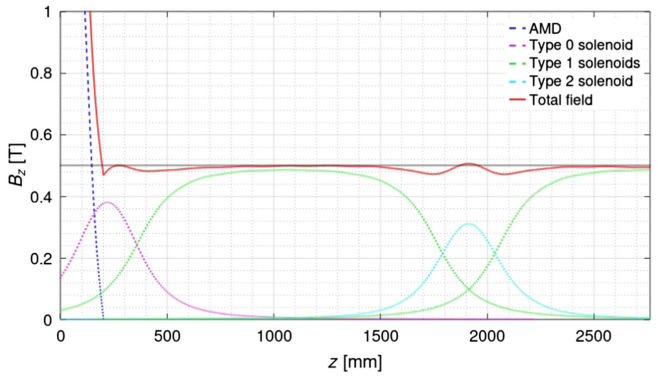

FIG. 10. Total on-axis magnetic field of the AMD and the NC solenoids. A breakdown of the total field is also displayed. Plot ranges are limited for a better display.

To simplify the design, the solenoids are assumed to have the same length and aperture. The optimized layout of the NC solenoids, as well as the target, AMD and accelerating structures, is displayed in Fig. 9. The total on-axis magnetic field of the AMD and the NC solenoids is presented in Fig. 10.

E. Collimation-chicane

In the old studies, the collimation of electrons and photons from the target has never been studied and simulated. In the new simulations, we use a chicane with a collimator placed at the center of the chicane to remove the electrons and photons, based on the SuperKEKB positron chicane design [25]. rf-Track [17,18] is used to simulate the dipoles in the chicane, assuming a uniform vertical dipole magnetic field. The chicane is composed of four identical dipoles, with only different field directions. The horizontal aperture should be large enough to accommodate the beam with a large horizontal offset and beam size in the bending dipoles. The vertical aperture is usually much smaller limited by the dipole yokes. Therefore, the beam pipe is assumed to have a rectangular aperture shape. The beam pipe aperture is a bit larger at the center of the chicane than inside the dipoles, to make space for the collimator. The chicane parameters, as well as the collimator parameters, are summarized in Table V.

F. Injector linac

The injector linac (IL) is supposed to accelerate the positrons, as well as the electrons, from 200 MeV to 2.86 GeV. An existed design of the IL [5] is used in the study. The schematic layout is presented in Fig. 11. The IL is composed of five FODO lattice sections, with increasing focusing lengths. The total number of quadrupoles used is 143, including 16 quadrupoles used in the five matching sections. The same CLIC L-band structure as the PIL is used. rf-Track [17,18] is used to simulate the transport of positrons in the IL. The parameters of the FODO lattices are summarized in Table VI. The parameters of the rf accelerating structures that are common in all sections are summarized in Table VII. To simplify the design, the same rf gradient and phase are assumed for all rf structures.

TABLE V. Chicane and collimator parameters.

Parameter	Symbol	Unit	Value
Chicane			
Dipole length	l	mm	200
Reference energy	e_0	MeV	200
Bending angle	θ	deg	$4.8, -4.8, -4.8, 4.8$
Beam pipe aperture inside dipoles (total width)	D_x, D_y	mm	120, 50
Beam pipe aperture for collimator (total width)	D_x, D_y	mm	180, 60
Distance between chicane and other sections	d_0, d_4	mm	200, 200
Distance between dipoles	d_1, d_2, d_3	mm	160, 250, 160
Collimator			
Collimator length	l	mm	120
Offset of the aperture	x_0	mm	−30
Aperture (total width)	D_x, D_y	mm	60, 60

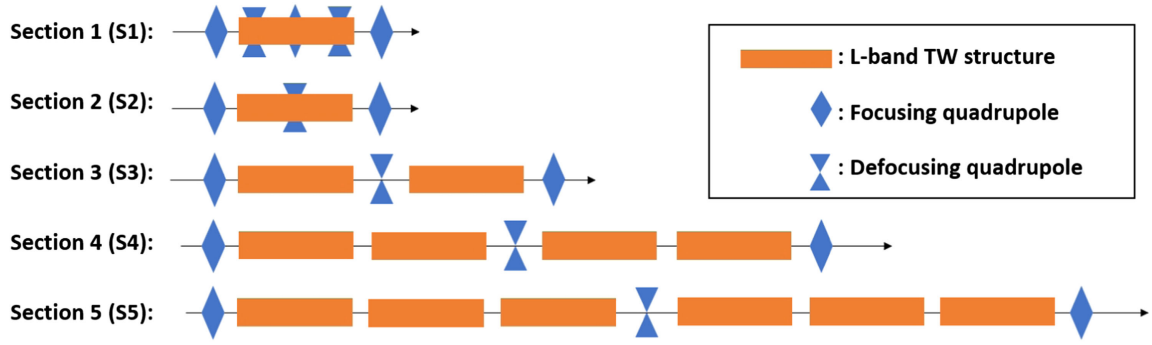

FIG. 11. Schematic layout of IL in five sections.

The matching sections as well as the rf gradients and phases are optimized for maximum PDR accepted positron yield.

G. Summary

A brief summary of the improvements in the design and simulation of the CLIC positron source compared with the old studies is as follows: (i) Target: The old hybrid target scheme is replaced with a new single target scheme with an optimized target thickness. As a result, the final positron yield is significantly increased and the deposited power is also significantly reduced. (ii) Primary electrons: The electron beam spot size has been optimized to achieve the maximum final positron yield below the required PEDD limit. As a result of yield improvement, the required electron bunch charge and beam power, inversely proportional to the final positron yield, are also significantly reduced. (iii) AMD: The old analytic field using the adiabatic formula is replaced with a realistic field from the realistic FC design. Positron yield overestimation in the old simulations with large AMD aperture is solved by using real aperture. (iv) NC solenoid: Constant on-axis field is replaced with analytic field from a more realistic design of the layout using three different types of solenoids. (v) Collimation: A chicane of four dipoles with a collimator placed at the center of the chicane is designed and used to collimate the electrons and photons from the target, which has never been studied before.

III. NOMINAL PERFORMANCE

The final results of the full simulation are summarized in Table VIII. Collective effects including the space charge and short-range wakefield are also considered in the simulation. The longitudinal phase spaces of the full simulation at the PDR entrance at the 380 GeV energy

TABLE VI. FODO lattice parameters of the IL in five sections (S1–S5).

Parameter	Symbol	Unit	S1	S2	S3	S4	S5
Total FODO cells	N_{FODO}		16	18	14	7	6
FODO lattice phase advance	μ	deg	90	90	90	90	90
Total quadrupoles	N_{Q}		33	37	29	15	13
Quadrupole length	l_{Q}	m	0.4	0.4	0.4	0.4	0.4
Spacing between quadrupoles	d	m	0.15	0.64	1.65	3.15	4.90
Quadrupoles surrounding a rf structure	n_{Q}		3	1	0	0	0
Total rf structures	N_{rf}		8	18	28	28	36

TABLE VII. Common rf structure parameters of the IL.

Parameter	Symbol	Unit	Value
rf frequency	f	GHz	2
rf structure length	l	m	1.5
rf structure aperture (radius)	a_0	mm	20
rf average gradient without compensation	G	MV/m	15.12
rf average gradient with compensation for short-range wakefield	G	MV/m	15.19
rf phase	φ	deg	0

TABLE VIII. Final results of the full simulation at different energy stages for different acceleration modes (DBA, drive beam-based acceleration and KBA, klystron-based acceleration).

Parameter	Unit	380 GeV		1.5 and 3 TeV
Acceleration mode		DBA	KBA	DBA
Optimized electron beam spot size	mm	2.40	2.45	1.50
Positron yield accepted by PDR		1.78	1.74	2.36
Required electron bunch charge	nC	0.56	0.43	0.30
Electron bunch charge assumed for collective effects	nC	0.8	0.6	0.4
Normalized electron beam power	kW	49.4	51.8	23.5
Normalized PEDD in target	J/g	33.1	33.2	32.8
Normalized total deposited power in target	kW	13.3	13.9	6.3

stage for the DBA acceleration mode are presented in Fig. 12. The PDR energy and time acceptance cut window as required in Table II is also displayed, with the position optimized for a maximum accepted positron yield inside the window. Compared with the fast simulation, although a loss of ∼12% is found in the PDR accepted positron yield with the full simulation, these are the best and most realistic simulation results that have ever been achieved for the CLIC positron source, as already discussed in Sec. II. Finally, a PDR accepted positron yield of $\tilde{1}.8$ is achieved at the 380 GeV energy stage and $\tilde{2}.4$ is achieved at higher energy stages. The PEDD in target is well controlled below 35 J/g. The required primary electron bunch charges are $\tilde{0}.6$ and $\tilde{0}.3$ nC at 380 GeV and higher energy stages, respectively, which are significantly smaller than the nominal bunch charge in the main linac, allowing for a possibility to reduce the electron beam energy, that is studied as an alternative option, as will be discussed in Sec. V.

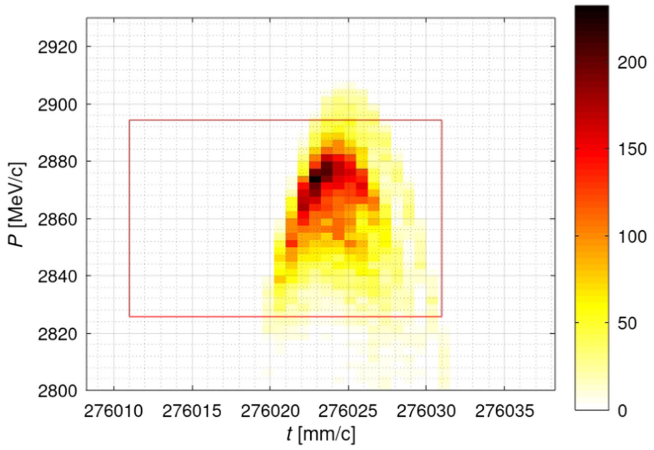

FIG. 12. Longitudinal phase spaces of the full simulation at the PDR entrance at the 380 GeV energy stage for the DBA acceleration mode. The PDR acceptance cut window is also displayed, with the position optimized for a maximum accepted positron yield inside the window.

IV. MISALIGNMENTS

The misalignment of the CLIC positron source has never been studied before, therefore, it is important to look at the impact on the final performance. The misalignments considered in the study are summarized in Table IX. All errors are given as rms values. A position error of 100 μm and an angular error of 100 μrad are assumed for all rf structures and magnets including the AMD, except for solenoids and dipoles that are short and more difficult to be aligned, in which case an angular error of 200 μrad is assumed. A strength error of 0.1% is assumed for all magnets. A gradient error of 1% and phase error of 0.1° are assumed for all rf structures. Besides, the positron beam from the target is assumed to have a position jitter error of 100 μm and an angular jitter error of 100 μrad.

The PDR accepted positron yield of the full simulation for 100 randomly misaligned machines at the 380 GeV energy stage for the DBA acceleration mode is presented in Fig. 13. Compared with the positron yield of the perfect machine without misalignments, the average yield of the misaligned machines is reduced by less than 6%, which is thought to be acceptable. Beam-based alignment corrections are not absolutely necessary but can be done to reduce the losses. Similarly, the normalized horizontal emittance is presented in Fig. 14. The performance of the vertical emittance is very similar and is, therefore, not presented. As a result, the average transverse emittances are also increased by less than 6%, which is acceptable. It is found

TABLE IX. Misalignments considered in the study. rms values are reported.

Misalignment	Unit	Value
Positron error for all elements	μm	100
Angular error for solenoids and dipoles	μrad	200
Angular error for other elements	μrad	100
Strength error for all magnets	%	0.1
rf gradient error for all structures	%	1
rf phase error for all structures	deg	0.1
Beam position jitter error	μm	100
Beam angular jitter error	μrad	100

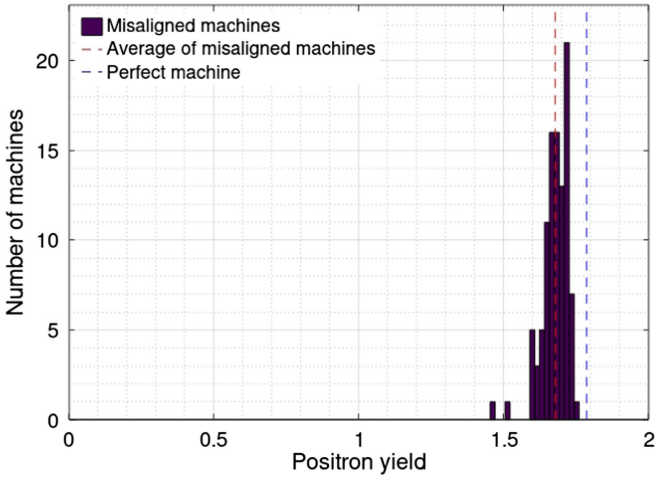

FIG. 13. PDR accepted positron yield of the full simulation for 100 randomly misaligned machines at the 380 GeV energy stage for the DBA acceleration mode.

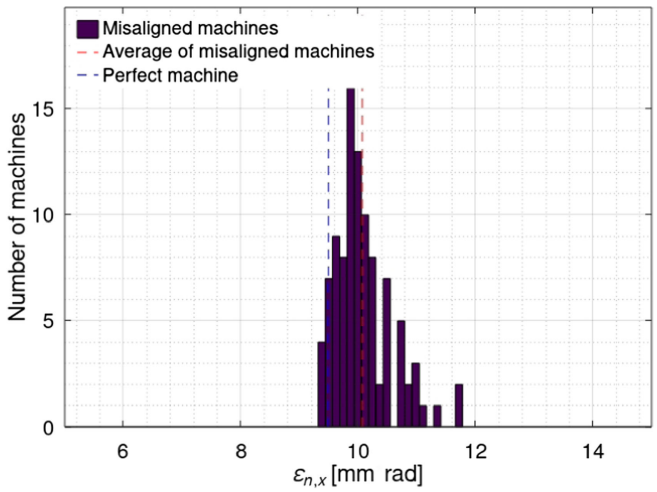

FIG. 14. Normalized horizontal emittance at the PDR entrance of the full simulation for 100 randomly misaligned machines at the 380 GeV energy stage for the DBA acceleration mode.

that the position error of the quadrupoles has the most significant impact on the final performance.

V. REDUCED ELECTRON BEAM ENERGY

It is obvious that a lower electron beam energy would reduce the linac length for the electron beam and the construction cost. The only problem is that the positron yield would also be reduced almost linearly, and a larger bunch charge would be required. In the baseline design, a 5 GeV electron beam is assumed, with a required bunch charge of the electron beam less than 0.6 nC, as seen in Table VIII. It seems possible to reduce the electron beam energy with a larger bunch charge. Therefore, a scan of the electron beam energy is performed to find the minimum

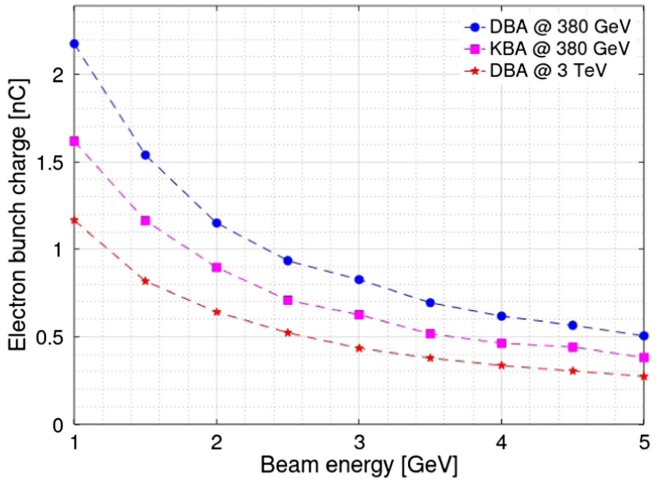

FIG. 15. Required primary electron bunch charge as a function of the electron beam energy at different energy stages for different acceleration modes.

energy. For each energy, the target thickness and the electron spot size are optimized separately. As a result, the required bunch charge and normalized total deposited power in the target are then plotted as a function of the electron beam energy at different energy stages for different acceleration modes, as presented in Figs. 15 and 16. The normalized total deposited power in the target is found to be reduced with a lower electron beam energy. The cooling of the target is also thought to be easier with a lower total deposited power. The normalized beam power is also found to be slightly reduced with a lower beam energy, though the scan is not presented. The operation cost of the electron linac is expected to be reduced with a lower beam power, while the construction cost of the linac is reduced with a lower beam energy. Therefore, it seems that the lower the

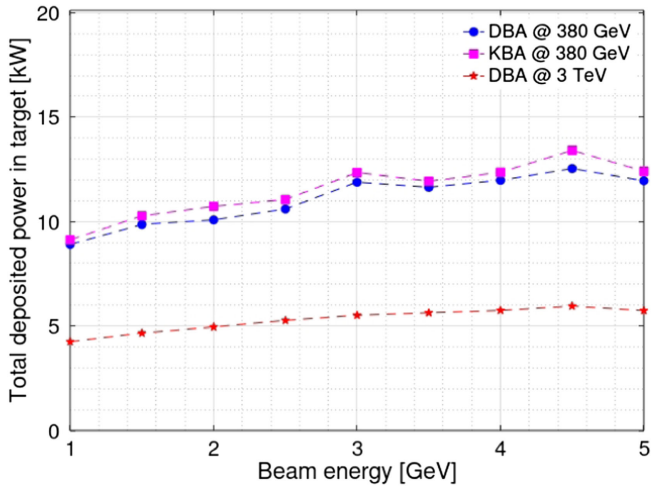

FIG. 16. Normalized total deposited power in the target as a function of the electron beam energy at different energy stages for different acceleration modes.

electron beam energy is, the better it is in cost saving and target cooling. However, the required electron bunch charge is increased significantly with a lower beam energy. Finally, it becomes a question of how much bunch charge can be accelerated with good beam quality in the electron linac. A good alternative option for the electron beam energy might be 2.3 GeV, which corresponds to a bunch charge of $\tilde{1}$ nC. Compared with the 5 GeV baseline, 2.3 GeV beam energy features: a shorter linac length, by a factor $\sim 5/2.3 \sim 2.2$; a beam power reduced by $\sim$10%; and a total deposited power in target reduced by 12.5%, as can be seen in the figures mentioned above. Nevertheless, this is a preliminary study of the possibility to reduce the energy, and more detailed studies are necessary if this proposal is to be achieved.

VI. CONCLUSIONS

The baseline design of the CLIC positron source has been updated with a start-to-end optimization at all collision energy stages, for both the drive beam-based and the klystron-based acceleration modes. In the optimized baseline, the hybrid target is replaced with a single amorphous tungsten target with the target thickness and electron spot size optimized. As a result, the final positron yield is significantly increased, and the electron bunch charge and beam power are significantly reduced. Compared with the most recently published optimization in 2019, the positron yield has been improved by a factor of 1.65, enabling the same reduction in the bunch charge and beam power of the primary electron beam. The total deposited power in the target is reduced by a factor of 2.1. The design, cooling, manufacturing, and mounting of the target will also be much easier and conservative. Final results of the most realistic simulations to date for the CLIC positron source are presented for the nominal configurations. In this case, the PDR accepted positron yield is about 1.8 for the first stage and 2.4 for higher energy stages, for a drive beam-based acceleration. The required electron bunch charge is about 0.6 and 0.3 nC correspondingly, while the electron beam power is about 49 and 24 kW. The impact of the misalignments and beam jitters is very important but has never been studied. In our simulations, it is found to be small and certainly acceptable. The average reduction in positron yield of 100 randomly misaligned machines with a jittered beam is less than 6%, while the average emittance growth is also less than 6%. The most significant impact on the performance is from the position error of the quadrupoles. Preliminary investigation of reducing the electron beam energy is presented. The optimization of the electron beam energy becomes a question of how much bunch charge can be accelerated with good beam quality in the electron linac. A good alternative option for the electron beam energy might be 2.3 GeV, which corresponds to a bunch charge of $\tilde{1}$ nC, and features shorter linac length, lower beam power and lower total deposited power in target, compared with the 5 GeV baseline. The construction and operation costs are, therefore, expected to be reduced accordingly with a shorter linac and a lower beam power. The cooling of the target is also expected to be easier with a lower total deposited power in target. The optimization methods and designs discussed in this report can be easily applied to many other collider positron source designs that require a high positron yield and a high-intensity positron beam. An example is the optimization of the Future Circular Collider (FCC) positron source, where we have done similar simulations and optimizations [26–29], and significant improvements have been achieved.

[1] M. Aicheler, P. Burrows, M. Draper, T. Garvey, P. Lebrun, K. Peach, N. Phinney, H. Schmickler, D. Schulte, and N. Toge, *A Multi-TeV Linear Collider Based on CLIC Technology: CLIC Conceptual Design Report*, CERN Yellow Reports, Monographs (CERN, Geneva, 2012), 10.5170/CERN-2012-007.

[2] M. Aicheler *et al.*, *The Compact Linear Collider (CLIC)—Project Implementation Plan*, edited by M. Aicheler, CERN Yellow Reports: Monographs (CERN, Geneva, 2018), p. 247, 10.23731/CYRM-2018-004.

[3] H. Bajas, S. Doebert, A. Latina, and Y. Zhao, Flux concentrator optimization for future positron sources, IEEE Trans. Appl. Supercond. **32**, 1 (2022).

[4] E. Darvish Roknabadi and S. Döbert, TW-structure design and E-field study for CLIC booster linac, Report No. CERN-ACC-2016-142, 2016, 10.18429/JACoW-IPAC2016-THPOR037, THPOR037.

[5] C. Bayar, A. K. Ciftci, S. Doebert, and A. Latina, Design and optimisation of the positron production chain for CLIC from the target to the damping ring, Nucl. Instrum. Methods Phys. Res., Sect. A **869**, 56 (2017).

[6] S. Agostinelli *et al.*, Geant4-a simulation toolkit, Nucl. Instrum. Methods Phys. Res., Sect. A **506**, 250 (2003).

[7] J. Allison *et al.*, Geant4 developments and applications, IEEE Trans. Nucl. Sci. **53**, 270 (2006).

[8] J. Allison *et al.*, Recent developments in Geant4, Nucl. Instrum. Methods Phys. Res., Sect. A **835**, 186 (2016).

[9] X. Artru, A simulation code for channeling radiation by ultrarelativistic electrons or positrons, Nucl. Instrum. Methods Phys. Res., Sect. B **48**, 278 (1990).

[10] O. Dadoun *et al.*, An event generator for crystal source application of the CLIC positron baseline, J. Phys. Conf. Ser. **357**, 012024 (2012).

[11] V. N. Baier and V. M. Katkov, Quasiclassical theory of Bremsstrahlung by relativistic particles, Sov. Phys. JETP **28**, 807 (1969), http://www.jetp.ras.ru/cgi-bin/e/index/e/28/4/p807?a=list.

[12] V. N. Baier, V. M. Katkov, and V. M. Strakhovenko, Electromagnetic cascades developing along crystal axes, Nucl. Instrum. Methods Phys. Res., Sect. B **119**, 131 (1996).

[13] A. I. Sytov, V. V. Tikhomirov, and L. Bandiera, Simulation code for modeling of coherent effects of radiation gen-

eration in oriented crystals, Phys. Rev. Accel. Beams, **22**, 064601 (2019).

[14] A. Sytov, L. Bandiera, and K. Cho *et al.*, Geant4 simulation model of electromagnetic processes in oriented crystals for accelerator physics, J. Korean Phys. Soc. **83**, 132 (2023).

[15] M. Soldani *et al.*, Radiation in oriented crystals: Innovative application to future positron sources, Nucl. Instrum. Methods Phys. Res., Sect. A **1058**, 168828 (2024).

[16] Y. Zhao, A. Latina, S. Doebert, D. Schulte, and L. Ma, Optimisation of the CLIC positron source at the 1.5 TeV and 3 TeV stages, CERN, Geneva, Reports No. CERN-ACC-2020-0026, No. CLIC-Note-1165, 2020, https://cds.cern.ch/record/2735292.

[17] A. Latina, *RF-Track Reference Manual* (CERN, Geneva, Switzerland, 2021), 10.5281/zenodo.4580369.

[18] A. Latina, in *The Tracking Code RF-Track and Its Application* (JACoW, Geneva, Switzerland, 2024), pp. 245–248, 10.18429/JACoW-HB2023-WEA3C1.

[19] Y. L. Han, C. Bayar, A. Latina, S. Doebert, D. Schulte, and L. L. Ma, Optimization of the CLIC positron source using a start-to-end simulation approach involving multiple simulation codes, Nucl. Instrum. Methods Phys. Res., Sect. A **928**, 83 (2019).

[20] Y. Morikawa, Development of ILC E-driven positron target, in *Proceedings of the 2024 International Workshop on Future Linear Colliders (LCWS24), Tokyo, Japan* (2024), https://agenda.linearcollider.org/event/10134/contributions/54842/.

[21] R. Chehab, G. Le Meur, B. Mouton, and M. Renard, An adiabatic matching device for the orsay linear positron accelerator, IEEE Trans. Nucl. Sci. **30**, 2850 (1983).

[22] A. V. Kulikov, S. D. Ecklund, and E. M. Reuter, SLC positron source pulsed flux concentrator, in *Proceedings of the 1991 IEEE Particle Accelerator Conference* (IEEE, New York, 1991), Vol. 3, pp. 2005–2007, 10.1109/PAC.1991.164851.

[23] OPERA-2D, Vector Fields Ltd. [Online]. Available: http://www.vectorfields.com/.

[24] P. Martín-Luna, B. Gimeno, D. González-Iglesias, D. Esperante, C. Blanch, N. Fuster-Martínez, P. Martinez-Reviriego, and J. Fuster, On the magnetic field of a finite solenoid, IEEE Trans. Magn. **59**, 1 (2023).

[25] T. Kamitani *et al.*, SuperKEKB positron source construction status, in *Proceedings of the 5th International Particle Accelerator Conference, Dresden, Germany* (JACoW, Geneva, Switzerland, 2014), MOPRI004, 10.18429/JACoW-IPAC2014-MOPRI004.

[26] Y. Zhao *et al.*, Comparison of different matching device field profiles for the FCC-ee positron source, in *Proceedings of the 12th International Particle Accelerator Conference, Campinas, SP, Brazil* (JACoW, Geneva, Switzerland, 2021), pp. 2617–2620, 10.18429/JACoW-IPAC2021-WEPAB015.

[27] Y. Zhao *et al.*, Positron capture simulations of the FCC-ee positron source, in *Proceedings of the FCC Week 2022, Paris, France* (2022), https://indico.cern.ch/event/1064327/contributions/4883171/.

[28] Y. Zhao *et al.*, Optimisation of the FCC-ee positron source using a HTS solenoid matching device, in *Proceedings of the 13th International Particle Accelerator Conference (IPAC'22), Bangkok, Thailand* (JACoW, Geneva, Switzerland, 2022), pp. 2003–2006, 10.18429/JACoW-IPAC2022-WEPOPT062.

[29] Y. Zhao *et al.*, FCC-ee positron capture system simulation, in *Proceedings of the FCC-ee Pre-Injector: CHART Collaboration Meeting, Frascati, Italy* (2023), https://agenda.infn.it/event/34369/contributions/194478/.